Nanoscopic Ultrafast Space-Time-Resolved Spectroscopy

T. Brixner,[1] F. J. García de Abajo,[2] J. Schneider,[1] and W. Pfeiffer[1]
[1]*Physikalisches Institut, Universität Würzburg, Am Hubland, 97074 Würzburg, Germany*
[2]*Centro Mixto CSIC-UPV/EHU and DIPC, Apartado 1072, 20080 San Sebastián, Spain*
(Received 22 September 2004; published 24 August 2005)

We propose and analyze a scheme for ultrafast spectroscopy with nanometer spatial and femtosecond temporal resolution. The interaction of polarization-shaped laser pulses with a nanostructure allows us to control the spatial and temporal evolution of the optical near field. Employing a learning algorithm, the field is tailored such that pump and probe excitation occur at different positions and at different times. Both excitations can be restricted to subdiffraction extensions and are separable on a nanometer length scale. This enables the direct spatial probing of nanoscale energy transfer or charge transfer processes.

DOI: 10.1103/PhysRevLett.95.093901 PACS numbers: 42.65.Re, 78.47.+p, 78.67.−n, 82.53.−k

Time-resolved optical measurements can be performed with a temporal resolution down to the femtosecond range, only limited by the duration of the laser pulses. However, the lateral spatial resolution is limited by diffraction to several hundred nanometers. Near-field effects can be used to minimize the excitation volume and allow a lateral resolution on the nanometer scale, as, e.g., has been demonstrated in two-photon fluorescence experiments [1]. Nevertheless, this optical near-field localization [1], the development of local detectors [2], or the technique of tuning in to spatially localized spectral resonances [3] represent only the first steps towards spatially and temporally resolved spectroscopy.

The most general objective for a nanoscopic ultrafast space-time-resolved spectroscopy is illustrated in Fig. 1(a). Consider two quantum systems separated by $\Delta x < 200$ nm, acting as local light absorbers. This situation occurs, for example, in photoactive macromolecules (e.g., light-harvesting pigment-protein complexes) or nanostructured systems such as quantum-dot assemblies. We are interested in monitoring charge transfer (CT) or energy transfer (ET) between the two systems. Therefore, we would like to excite the first subsystem locally at position $\mathbf{r}_1$ and time t_1 with an ultrashort interaction of $\tau \approx 20$ fs duration, and then to probe the second subsystem some time $\Delta t \sim 0 \ldots 1000$ fs later at location $\mathbf{r}_2$. Following excitation at $(\mathbf{r}_1, t_1)$ and CT or ET within the time interval Δt, an excited state is present at $(\mathbf{r}_2, t_2)$ and can be detected, for example, via photoemission. In this way, the temporal signature of CT or ET can be measured directly in the photocurrent. This requires subdiffraction spatial resolution on the order of $d \approx 20$ nm and the possibility of independently controlling the field evolution at the two locations $\mathbf{r}_1$ and $\mathbf{r}_2$. This would not work with conventional light fields, because there, the minimal focused spot size is on the order of the wavelength and separate excitations of the two subsystems would not be possible. Hence, conventional techniques realize either the required time resolution (femtosecond pump-probe) or the desired subdiffraction spatial resolution (near-field optics), but not both. In this Letter, we propose and analyze a method which allows us to tailor independently the spatial and temporal evolution of the electric field distribution in order to meet the conditions indicated in Fig. 1(a).

The two basic ingredients of our scheme are adaptive femtosecond polarization laser pulse shaping [4] and optical near-field distributions of metal nanostructures. Femtosecond pulse shaping is used in many applications in quantum control [5,6], and the specific properties of the ultrafast variation of light polarization have also been recently exploited [7–10]. Optical near fields, on the other hand, have a number of applications [1,11–14] based on the following properties: subwavelength variation of the field strength, local field enhancement with respect to the incident wave, and longitudinal field vector components. Recently, we have shown how to control all three polarization components of the local electric field vector at a particular location [15]. Here, however, we use polarization shaping to create electric fields with *specific spatial and temporal* characteristics such that the properties depicted in Fig. 1(a) are realized. The task to achieve an electric field with the desired characteristics is performed by a learning algorithm [16]. The polarization state of an incident laser pulse is represented by the spectral intensities $I_i(\omega)$ and phases $\varphi_i(\omega)$ for two orthogonal polarization components $i = 1$ and $i = 2$. In our simulations we use Gaussian spectra (central frequency $\omega = 2.46\ \mathrm{rad\,fs^{-1}}$, FWHM $= 0.23\ \mathrm{rad\,fs^{-1}}$) and 128 frequency sampling points for both components.

We solve the frequency-dependent Maxwell equations rigorously for a given nanostructure and incidence angle by means of the boundary-element method [17,18] using the measured bulk dielectric functions [19] to describe the local response of the involved material. In this Green's function approach, equivalent surface charges and currents are introduced to account both for external sources and induced sources. For discretized surfaces this reduces the problem to a set of integral equations that are solved self-consistently. Propagation/retardation effects are incorporated. We obtain the local spectral response in the form of complex-valued matrices $A^i_\alpha(\mathbf{r}, \omega)$, where $\alpha = x, y, z$ indicates the component of the electric field at point $\mathbf{r}$ and

frequency ω induced by a far field of linear polarization $i = 1$ or $i = 2$. The amplitude $|A^i_\alpha(\mathbf{r}, \omega)|$ describes the extent to which the two far-field components 1 and 2 couple to the local field, whereas the phase $\arg\{A^i_\alpha(\mathbf{r}, \omega)\}$ establishes their correct vectorial superposition. Because of the linearity of Maxwell's equations, the total local field is then obtained as

$$\mathbf{E}(\mathbf{r}, \omega) = \sum_{i=1}^{2} \begin{pmatrix} A^i_x(\mathbf{r}, \omega) \\ A^i_y(\mathbf{r}, \omega) \\ A^i_z(\mathbf{r}, \omega) \end{pmatrix} \sqrt{I_i(\omega)} e^{i\varphi_i(\omega)}, \qquad (1)$$

and the local field in the time domain $\mathbf{E}(\mathbf{r}, t)$ by separately Fourier transforming each vector component of $\mathbf{E}(\mathbf{r}, \omega)$.

The demonstration of spatial and temporal "focusing" of the field distribution on a nanometer and femtosecond scale requires localizing the light intensity at certain points $\mathbf{r}_j$ *and* at specific times t_j. This objective is expressed in terms of a fitness function

$$f = \sum_j \int_{-\infty}^{\infty} \left[\left(\sum_\alpha a_\alpha E^2_\alpha(\mathbf{r}_j, t) \right) \times \left(\sum_\alpha a_\alpha E^2_\alpha(\mathbf{r}_j, t_j) \right)^{-1} - p_j(t) \right]^2 dt,$$
$$\alpha = x, y, z, \qquad j = 1, 2, 3 \ldots, \qquad (2)$$

where a_α are coefficients that determine which field components are optimized and $p_j(t)$ reflects the desired time dependence of the normalized intensity at point $\mathbf{r}_j$. The temporal target function $p_j(t)$ is composed of a normalized Gaussian distribution with its maximum at time t_j and an FWHM of τ_j. The fitness function can be interpreted as the squared deviation of the field intensity $\Sigma_\alpha a_\alpha E^2_\alpha(\mathbf{r}_j, t)$ from the target $p_j(t)$, summed over all investigated points $\mathbf{r}_j$ and times t_j. The factor $[\Sigma_\alpha a_\alpha E^2_\alpha(\mathbf{r}_j, t_j)]^{-1}$ normalizes the intensity to its value at the desired peak position t_j. Minimization of f by an evolutionary algorithm [16] that adjusts the spectral phases $\varphi_i(\omega)$ of the two input polarization components leads to a field distribution which is as close as possible to the desired behavior illustrated in Fig. 1(a). The optimum is reached after typically 300 generations, and repetitive optimizations yield the same final fitness and almost identical $\varphi_i(\omega)$.

For an illustration of this method, we choose the model nanostructure shown in Fig. 1(b), i.e., an Ag tip positioned above a nanometer sized Ag sphere of 25 nm radius, which is illuminated by polarization-shaped plane waves. The apex of the conical Ag tip with an opening angle of 5°, a tip radius of 10 nm, and a total length of 1500 nm, is located 5 nm above the sphere surface. The incidence plane is the x-z plane and the incidence angle is 45° with respect to the x axis. Polarization component 1 lies in the x-z plane and component 2 is parallel to the y axis. As indicated in Figs. 2(a) and 2(b) the chosen nanostructure exhibits no pronounced spectral features. Thus, the response time is very fast and plasmon resonances play only a minor role [20]. The goal for field control was now to achieve a high intensity E^2_x of the x component of the local electric field vector ($a_y = a_z = 0$ in f) at point $\mathbf{r}_1 = (-30, 30, 27.5)$ nm and time $t_1 = 0$ fs as well as a high intensity of E^2_x at point $\mathbf{r}_2 = (-30, -30, 27.5)$ nm at a later time $t_2 = 40$ fs with near-field pulse durations $\tau_1 = \tau_2 = 15$ fs, but low intensity at all other times. The complex shapes of the optimized spectral phases $\varphi_1(\omega)$ and $\varphi_2(\omega)$ [Fig. 2(c)] illustrate that the solution to this problem is not trivial. Differences between the two polarization components indicate that polarization shaping is important.

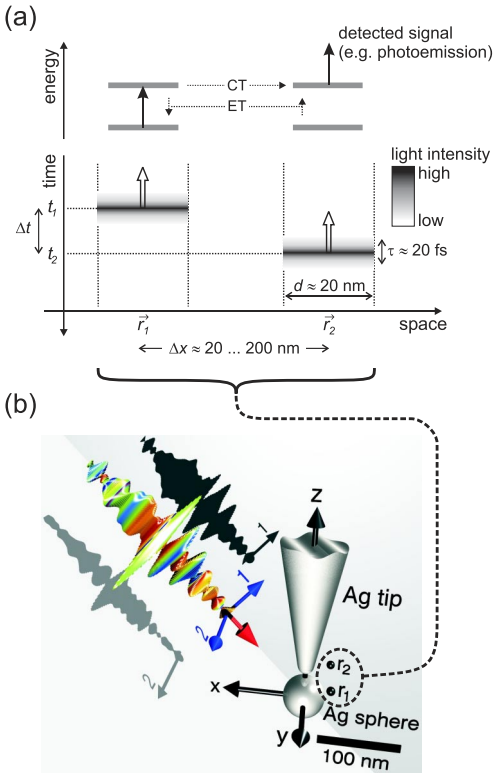

FIG. 1 (color online). Ultrafast space-time-resolved spectroscopy. (a) Objective: To study charge transfer (CT) or energy transfer (ET) between two quantum systems that are only a short distance Δx apart, we create electromagnetic fields with the characteristics shown. The interaction of light with the quantum systems occurs only in spatially limited places with subdiffraction resolution d and femtosecond time resolution τ. Variation of the time delay Δt opens the prospect for space-time-resolved spectroscopy on the nanoscale. For example, the field first creates local excitation at $\mathbf{r}_1$, and later the transferred excitation is detected at $\mathbf{r}_2$, e.g., by photoelectron emission. (b) Proposed scheme: The model nanostructure is illuminated by an optimized polarization-shaped femtosecond laser pulse. The coordinate systems for the nanostructure and for the polarization state of the laser pulse are indicated by arrows. The optimal polarization-shaped laser pulse corresponding to Fig. 3(b) is shown using an intuitive representation [23], where the ellipses indicate the momentary time-dependent polarization state and amplitude of the electric field oscillations. The gray-shading (color online) shows the momentary oscillation frequency, whereas the shadows represent the amplitude envelopes of components 1 and 2 separately.

Figure 2(d) shows the resulting temporal intensity evolution of the near field at points $\mathbf{r}_1$ (solid line) and $\mathbf{r}_2$ (dashed line), while Fig. 2(e) illustrates the spatial-temporal evolution as a contour plot. Indeed, at $t = 0$ fs the intensity E_x^2 peaks at point $\mathbf{r}_1$ whereas at $\mathbf{r}_2$ it reaches only about 20% of its maximum value and vice versa at $\mathbf{r}_2$ the intensity E_x^2 peaks at 40 fs. As seen in the contour plot of $E_x^2(t)$ along a straight line given by $x = -30$ nm and $z = 27.5$ nm [Fig. 2(e)], the maximum of the field distribution clearly shifts from positive y coordinates at $t = 0$ fs to the negative side 40 fs later. The spatial spreading of the field localization, i.e., the spatial resolution d, is about 30 nm in the y direction reflecting the spatial extension of the near-field modes, and of similar magnitude along the x direction. Overall, this means that indeed we have succeeded in creating an electric field with the characteristics described in Fig. 1(a). The restriction on the x component of the field can be interpreted as an excitation and probing of transitions with dipole moments oriented along the x direction and does not reflect a limitation of the proposed scheme. Using a slightly different illumination geometry and a gold nanostructure (results not shown), we have successfully controlled the total intensity.

The simultaneous spatial and temporal field control opens the door to new types of spectroscopy with ultrahigh temporal and spatial resolution. We have verified that the pump-probe delay time can be varied at will within the temporal window of the pulse shaper [Fig. 3(a)]. The basic strategy for performing this type of spectroscopy is thus: First, calculate the required external polarization-shaped laser field for a particular delay time and spatial separation in a learning loop; second, apply these settings to the pulse shaper, illuminate the nanostructure [Fig. 1(b)], and record the experimental signal (e.g., photoelectron current); then, repeat this procedure for all desired delay times. Note that we do not need separate pump and probe laser beams. Rather, the complete spatial-temporal pump-probe field is already generated by a single polarization-shaped input pulse. In this scheme, our objective is not to study the physics of the tip-sphere assembly but merely to use it as a tool for space-time-resolved spectroscopy on another system that is brought into its vicinity.

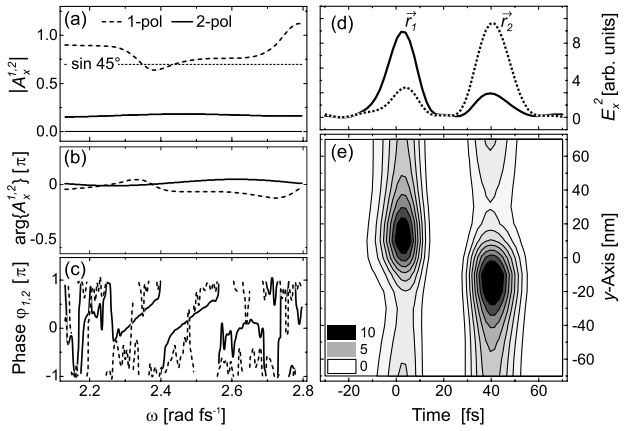

FIG. 2. Spatiotemporal field control. The spectral response $A_x^{1,2}(\mathbf{r}_2, \omega)$ for the x component of the local electric field under excitation with 1-polarized (thick dashed line) or 2-polarized light (thick solid line), respectively, is given as (a) amplitude $|A_x^{1,2}|$ and (b) phase $\arg\{A_x^{1,2}\}$. The far-field amplitude is shown in (a) by a horizontal line. The far-field spectral phases (c) of an optimally polarization-shaped laser pulse yield the temporal spatial intensity evolution of the x component of the local electric field shown in (d) and (e). Part (d) shows the intensity evolution at $\mathbf{r}_1 = (-30, 30, 27.5)$ nm (solid line) and at $\mathbf{r}_2 = (-30, -30, 27.5)$ nm (dashed line) in the geometry of Fig. 1(b). The temporal evolution of the intensity E_x^2 in arbitrary units along the straight line defined by $\mathbf{r}_1$ and $\mathbf{r}_2$ is shown in (e) as contour plot.

We emphasize that the spatial resolution of the proposed spectroscopy does not rely on a high spatial resolution of the detection method; it is rather already intrinsic to the whole near-field scheme as seen in Fig. 2. However, the signal-to-background ratio can be improved either by using detection methods with high spatial resolution or by using local resonances. For example, the local detection of a multiphoton-induced photoelectron signal has been demonstrated with some 10 nm resolution [21] and therefore should be also feasible here.

Other schemes for space-time-resolved spectroscopy are conceivable. For instance, it is possible to modify the duration of the two local excitations independently (e.g., in Fig. 3(b) for delay $\Delta t = 0$). This configuration could be useful especially if probe signals other than photoelectron emission, such as second-harmonic generation, are used. The long interaction at $\mathbf{r}_1$ with corresponding low intensity avoids a strong nonlinear signal from the pump excitation alone. On the other hand, the short interaction at $\mathbf{r}_2$ with corresponding high intensity generates a nonlinear signal that depends on the local state of the quantum system at $\mathbf{r}_2$. A modulation of this signal would thus reflect, for ex-

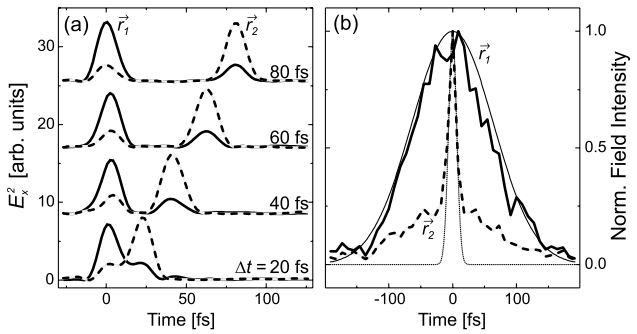

FIG. 3. (a) Nanoscale pump probe. The temporal intensity of the x component of the local electric field is shown for different pump-probe delays at $\mathbf{r}_1$ (solid) and at $\mathbf{r}_2$ (dashed), displaced vertically for clarity. (b) Nanoscale pump probe with different pulse durations. The evolution of the normalized total electric field intensity at $\mathbf{r}_1$ and at $\mathbf{r}_2$ is shown by thick solid and dashed lines, respectively. The corresponding temporal target functions are shown as thin lines; the optimized external polarization-shaped laser pulse is shown in Fig. 1(b).

ample, the transfer or localization of energy deposited at $\mathbf{r}_1$. Note that the temporal separation between both maxima can be adjusted and hence the spatial dynamics can be studied in a time-resolved fashion.

The main mechanism of spatiotemporal field control is constructive versus destructive interference of near-field modes. In the far field the two electric field components 1 and 2 are perpendicular to each other and therefore do not interfere. However, the local fields $\mathbf{E}_1(\mathbf{r})$ and $\mathbf{E}_2(\mathbf{r})$ generated by the external polarization components 1 and 2, respectively, are in general no longer perpendicular and therefore interfere at least partially. This interference then depends on the phase difference between the two components $i = 1$ and $i = 2$, thus leading to enhancement or suppression of the near field $\mathbf{E}(\mathbf{r}, \omega)$ at specific positions. This identification of the control mechanism is confirmed by the observation that spatiotemporal fields such as in Fig. 1(a) cannot be achieved by pulse shaping of linearly polarized light (results not shown). Hence, the main mechanism here differs from the linear chirp effect recently demonstrated by Stockman *et al.* [22]. Anisotropic spectral resonances can be excluded as control mechanism because of the flat response of the model nanostructure [Figs. 2(a) and 2(b)]. Hence, interference as accessed by polarization shaping is essential to create nanoscale spatial-temporal pump-probe sequences.

Apart from these prospects for space-time-resolved ''nanofemto'' spectroscopies, there are other potential applications of the near-field control scheme. The chosen model nanostructure resembles the standard geometry in many scanning probe techniques. Accordingly, the illumination of scanning probe tips with polarization-shaped laser pulses could also be used (i) to spatially focus the near-field distribution, (ii) to scan the optical excitation with respect to the tip position without mechanical movement, and (iii) to optimize the response in nonlinear optical scanning probe techniques such as scanning two-photon fluorescence microscopy [1]. Another interesting application of space-time controlled near fields is the realization of novel quantum control schemes in which the three-dimensionally shaped electric fields vary on the length scale of quantum wave functions.

It is important to note that the demonstrated scheme is not limited to the particular tip-sphere geometry or the locations $\mathbf{r}_1$ and $\mathbf{r}_2$ chosen here. The described control mechanism will work with any nanostructure if the two polarization components couple to interfering near-field modes and if the local responses with respect to the two input polarization components are different at the desired spatial locations.

Summarizing, polarization pulse shaping can be used to simultaneously control the spatial and temporal evolution of optical near-field distributions. The dominant control mechanism is based on two-pathway interference between the modes excited by the two incident polarization components. The choice of the appropriate time-dependent polarization of the illuminating laser is not trivial and hence a learning algorithm was applied for automated optimization. We demonstrated how such light fields open the route toward space-time-resolved spectroscopies below the diffraction limit, in which pump and probe excitations can be located simultaneously and independently on a nanometer length scale and femtosecond time scale using a single laser pulse.

T. B. thanks the German Science Foundation for financial support. F. J. G. A. acknowledges help and support from the Spanish MEC (FIS2004-06490-C03-02).

[1] E. J. Sanchez, L. Novotny, and X. S. Xie, Phys. Rev. Lett. **82**, 4014 (1999).
[2] M. Merschdorf, W. Pfeiffer, A. Thon, and G. Gerber, Appl. Phys. Lett. **81**, 286 (2002).
[3] V. Sundström, T. Pullerits, and R. van Grondelle, J. Phys. Chem. B **103**, 2327 (1999).
[4] T. Brixner and G. Gerber, Opt. Lett. **26**, 557 (2001).
[5] S. A. Rice and M. Zhao, *Optical Control of Molecular Dynamics* (Wiley, New York, 2000).
[6] T. Brixner and G. Gerber, Chem. Phys. Chem. **4**, 418 (2003).
[7] D. Oron, N. Dudovich, and Y. Silberberg, Phys. Rev. Lett. **90**, 213902 (2003).
[8] N. Dudovich, D. Oron, and Y. Silberberg, Phys. Rev. Lett. **92**, 103003 (2004).
[9] T. Suzuki, S. Minemoto, T. Kanai, and H. Sakai, Phys. Rev. Lett. **92**, 133005 (2004).
[10] T. Brixner, G. Krampert, T. Pfeifer, R. Selle, G. Gerber, M. Wollenhaupt, O. Graefe, C. Horn, D. Liese, and T. Baumert, Phys. Rev. Lett. **92**, 208301 (2004).
[11] K. Kneipp, Y. Wang, H. Kneipp, L. T. Perelman, I. Itzkan, R. Dasari, and M. S. Feld, Phys. Rev. Lett. **78**, 1667 (1997).
[12] S. R. Emory and S. M. Nie, Anal. Chem. **69**, 2631 (1997).
[13] T. W. Ebbesen, H. J. Lezec, H. F. Ghaemi, T. Thio, and P. A. Wolff, Nature (London) **391**, 667 (1998).
[14] M. Quinten, A. Leitner, J. R. Krenn, and F. R. Aussenegg, Opt. Lett. **23**, 1331 (1998).
[15] T. Brixner, W. Pfeiffer, and F. J. García de Abajo, Opt. Lett. **29**, 2187 (2004).
[16] T. Baumert, T. Brixner, V. Seyfried, M. Strehle, and G. Gerber, Appl. Phys. B **65**, 779 (1997).
[17] F. J. García de Abajo and A. Howie, Phys. Rev. Lett. **80**, 5180 (1998).
[18] F. J. García de Abajo and A. Howie, Phys. Rev. B **65**, 115418 (2002).
[19] E. D. Palik, *Handbook of Optical Constants of Solids* (Academic, New York, 1997).
[20] M. Merschdorf, C. Kennerknecht, and W. Pfeiffer, Phys. Rev. B **70**, 193401 (2004).
[21] M. Bauer and M. Aeschlimann, J. Electron Spectrosc. Relat. Phenom. **124**, 225 (2002).
[22] M. I. Stockman, S. V. Faleev, and D. J. Bergman, Phys. Rev. Lett. **88**, 067402 (2002).
[23] T. Brixner, G. Krampert, P. Niklaus, and G. Gerber, Appl. Phys. B **74**, S133 (2002).